

Olivine-Pyroxene Distribution of S-type Asteroids Throughout the Main Belt

Shaye Storm

IfA REU 2007 and Massachusetts Institute of Technology

Advisor: Schelte J. Bus

Received _____; accepted _____

ABSTRACT

The mineralogical composition of asteroids can be constrained using visible and near-IR (VNIR) spectroscopy. The most prominent spectral features observed over this wavelength range are due to olivine and pyroxene, the two most abundant minerals in both chondritic and achondritic meteorites. The observed ratio of these two minerals is highly dependent on the amount of heating that an asteroid has undergone. The 1-micron band minimum and the band area ratio (BAR) between the 2- and 1-micron bands reveal the relative abundance of olivine and/or pyroxene on an asteroid surface (Gaffey 1993). A large sample of S-, A-, V-, and R-type asteroid spectra was collected over the visible and near-IR wavelengths. Here we present a methodology for calculating the location of the 1-micron band minimum and BAR with appropriate 1- sigma uncertainties. This method was used to characterize approximately 200 S-type asteroids throughout the main belt. We will also present the distribution of olivine / pyroxene throughout the main belt by measuring how the S-type mineralogy varies with heliocentric distance. This will provide a better understanding of both the thermal processing across the main belt and subsequent mixing of asteroids through collisional and dynamical processes.

1. Introduction

1.1. Mineralogy

S-types are primarily composed of olivine and pyroxene. These minerals control the observed spectral features of asteroids. Pyroxene has absorption features located around 1-

and $2\text{-}\mu\text{m}$, while olivine has absorption features located around $1\text{-}\mu\text{m}$. These broad features are composed of higher resolution bands that are controlled by the physical structure of the mineral, and by the vacancies in the silicon-oxygen crystal structure. Fe^+ and Mg^+ are the primary ions that fill in the olivine vacancies, whereas Fe^+ , Mg^+ and Ca^+ fill in the pyroxene vacancies. Sunshine *et al.* have began the next step of mineralogical studies by using Modified Gaussian Modeling (MGM) to deconvolve the broad spectral features into the higher resolution bands controlled by the mineral vanancies, but this study focuses on the broader 1- and $2\text{-}\mu\text{m}$ bands.

1.2. Observations

The S-type spectra were obtained in the visible wavelengths from Phase II of the Small Main-Belt Spectroscopic Survey (SMASSII) (Bus and Binzel 2002). SMASSII used the 2.4-m Hiltner and 1.3-m McGraw Hill telescopes and had a wavelength range of $0.435\text{-}0.925\mu\text{m}$. Near-infrared data was obtained from continuing runs on NASAs Infrared Telescope Facility using SpeX with a wavelength range of $0.7\text{-}2.49\mu\text{m}$. The SpeX data was crucial for this study, since it included the 1- and $2\text{-}\mu\text{m}$ bands, which represent the mineral chemistry of the asteroids.

1.3. S-type Taxonomy

Starting with the Tholen classification (Tholen 1989), S-types were all lumped into one category. This taxonomy was based on the Eight-Color Asteroid Survey (ECAS). The SMASSII classification offered improved resolution in the visible wavelengths, and the S-types were subsequently broken down into 6 subtypes. The addition of the near-IR SpeX data allows mineralogy to be incorporated into the taxonomy. This next step puts physical

meaning behind the letters of taxonomy.

2. Methodology

2.1. Improvement of error bars

The original error bars warranted re-evaluation since a major goal of this study was to calculate appropriate error bars for the Band I Center. The original spectral error bars are only representative of random photon statistics. The varying systematic errors introduced to each channel through the telluric correction are unaccounted for, leading to under approximations of error. 400 spectra were spline fit to analyze this systematic error. The systematic error was defined as $(Observerd - Fit Reflectance)/(Photon Error)$. The mean and standard deviation of the systematic error for each wavelength was summed in quadrature to aquire the final error bar correction value. The new error bar values were the original error multiplied by the obtained systematic value for the appropriate wavelength (see Appendix for plot).

2.2. Band Area Ratio

The band area ratio (BAR) is one of the main spectral features used to determine the olivine-pyroxene relative abundance ratio. The band one and two area definitions were determined through laboratory experiments (Cloutis 1986): “The band I area is defined as the area enclosed by the spectral curve and a straight-line tangent to the relative maxima at 0.7 and 1.4-1.7 μm . The band II area is enclosed by the spectral curve and straight line fixed on the curve at 2.4 μm (because the absorption wing is incomplete) and the 1.4- to 1.7- μm maximum.” This traditional BAR definition was used with two slight modifications. First, it is not possible to determine the exact tangent lines (continuum line from now on)

to the spectral curve for both band areas. Fitting a line to the local maxima of the spectra is not the most accurate definition of the continuum line. A more improved estimate of the continuum was found by fitting the regions around the relative maxima with second order polynomials, and solving for the equation of the tangent lines to those polynomials. This gives a more robust approximation for the continuum, which is also important for calculating the Band I Center. Second, not all BII areas were cut off at $2.5\mu\text{m}$. If the spectrum had a relative maximum in the $2\text{-}2.5\mu\text{m}$ region, then the BII area was measured up to that maximum.

2.3. Band I Center

Calculating and defining the Band I Center is a very difficult task. It is important to remember that Band I is a convolution of absorption bands arising from distinct ion vacancies for olivine and pyroxene. The deconvolution of the band is currently being studied using the Modified Gaussian Method (MGM) (Sunshine 2007). The complexity of the band creates the difficulty of defining a band center when only looking at the convolved band. It is generally agreed that the absolute band minimum, attained from a high order polynomial fit, is not the desired feature. The broadness of a second order polynomial suits Band I for fitting since we are looking to track a broad structure. After choosing a second order polynomial, it is then crucial to define the sections of the band to fit. It is clear that the bottom of Band I often has a quadratic shape, but the rest of the band quickly diverges from quadratic to a higher order shape. Therefore, if the band is fit from small reflectance values all the way to the highest reflectance values, a lot of systematic error will be introduced. We found that fitting a second order polynomial over the bottom third of the band introduces little or no systematic error. The Band I Center was calculated in the following way. First, we set a reflectance upper limit just above the three lowest reflectance

points. Second, we fit a second order polynomial to the data and solved for the reflectance minimum and corresponding wavelength. Third, we resampled the reflectance values and repeated step two one hundred times. The resampled reflectance is:

$$\text{Reflectance} + \text{New Error} \times \text{Random number from Normal Distrib}(\text{mean} = 0, \sigma = 1)$$

Fourth, we increased the reflectance upper limit (i.e. increase the number of points in the band to fit). Fifth, we repeated steps two, three, and four until the reflectance upper limit reached one-third of the total band reflectance. We averaged all corresponding wavelengths to get a value for the Band I Center, and took the standard deviation of all the corresponding wavelengths to get a value for the Band I Center Error Bar.

3. Results

3.1. Mixing Line Distribution of 188 S-type Asteroids

The mixing line was developed by Cloutis (Cloutis 1986) as a tool to study the olivine-pyroxene abundance ratio in meteorites and asteroids. The majority of asteroids in this study fall along the mixing line in a predictable manner (see Appendix for plot): the Vestoids are in the pyroxene rich region, and the A-types are mostly found in the olivine rich region. The S-types exhibit clumping patterns; the clump around $0.98\mu\text{m}$ Band I Center might represent the ordinary chondrites as hypothesized by previous literature. The S-type families cluster along the mixing line while the background objects spread over the range of BAR and Band I Center. The Band I Center error bars average $0.00664\mu\text{m}$ and span $0.000870\mu\text{m} - 0.06184\mu\text{m}$.

3.2. Heliocentric Distance Distribution of 188 S-type Asteroids

Note that the 188 asteroids are not a random sample of the main belt. There was observational bias towards objects in spectro-dynamical families. At first glance, there does not seem to be obvious structure in the heliocentric distribution (see Appendix for plot). A running box-car average with 10 asteroids represented in each data point (family members were averaged into 1 data point before overall averaging) was done to smooth the data and look for any trends. There appears to be an overall trend of decreasing olivine/pyroxene ratio moving further away from the sun. This contradicts the first approximation that S-types closer to the sun should be more thermally altered.

4. Conclusions

The thermal trends found in the S-type asteroids seem to indicate a lower olivine/pyroxene content for asteroids in the outer region of the belt, compared to the inner belt asteroids. This trend would be important for our understanding of the cosmochemistry and dynamics of the main belt, and will need to be confirmed with further work. Crucial next steps will include adding more main belt asteroids. These asteroids will ideally be background objects not belonging to any known spectro-dynamical family. As the classification of asteroid families improves, so will the ability to properly select a random sample of the main belt.

REFERENCES

- Bell, J.F., David, D.R., Hartmann, W.K., Gaffey, M.J. (1989). Asteroids: The Big Picture. In *Asteroids II*, (R.P Binzel, T. Gehrels, M. Matthews, eds.), Univ. Arizona Press, pp 921-945.
- Bus, S.J., Binzel, R.P. (2002). Phase II of the Small Main-Belt Asteroid Spectroscopic Survey, The Observations. *Icarus* 158, 106-145.
- Cloutis, E. A., Gaffey, M. J., Jackowski, T.L., and Reed, K. L. (1986). Calibrations of phase abundance, composition, and particle size distribution for olivine-orthopyroxene mixtures from reflectance spectra. *JGR*, 91, 11641.
- Gaffey, M.J., *et al.* (1993). Mineralogical variations within the S-type asteroid class. *Icarus* 106, 573.
- Rayner, J. T., *et al.* (2003). SpeX: A Medium-Resolution 0.8-5.5 Micron Spectrograph and Imager for the NASA Infrared Telescope Facility. *PASP* 115, 362-382.
- Sunshine, J.M., *et al.* (2007). Olivine-dominated asteroids and meteorites: Distinguishing nebular and igneous histories. *MPS* 42, 155-170.
- Tholen, D.J. (1989). Asteroid Taxonomic Classifications. In *Asteroids II*, (R.P Binzel, T. Gehrels, M. Matthews, eds.), Univ. Arizona Press. pp 1139-1150.

A. Figures

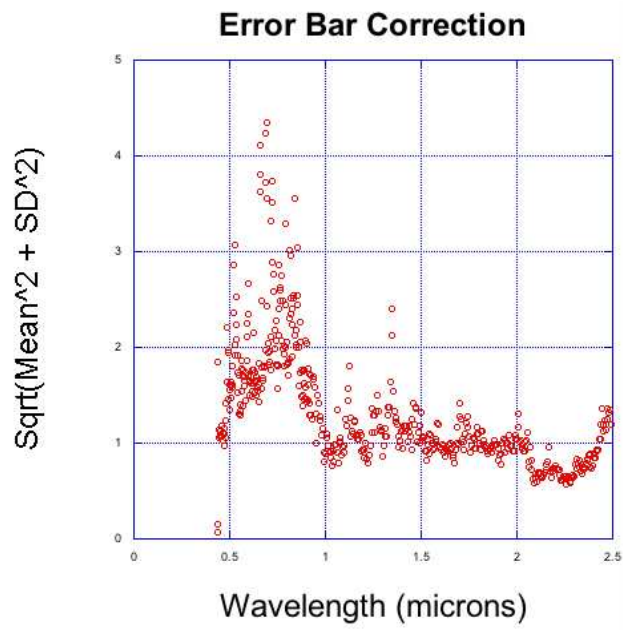


Fig. 1.— This plot shows the systematic error introduced by the telluric correction at each wavelength.

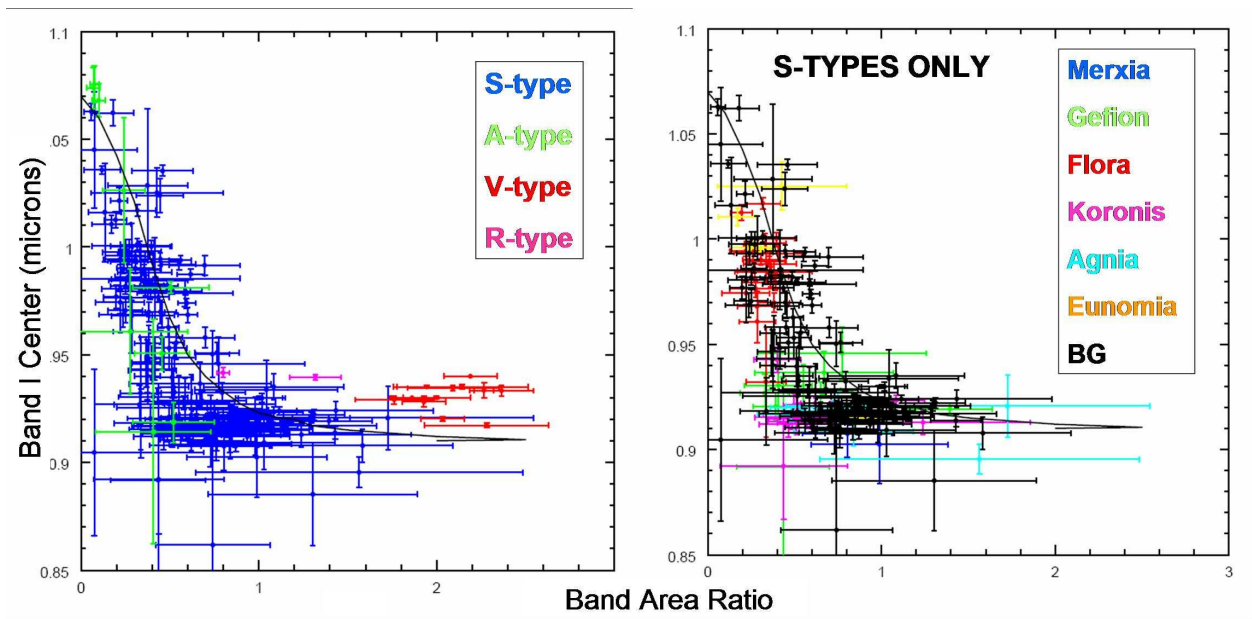


Fig. 2.— Mixing Line Distribution. The left plot shows all asteroids. The right plot shows only S-types divided by family (BG=background asteroids). The asteroids all fall along the mixing line as expected. The Band I Center error bars average $0.00664\mu\text{m}$.

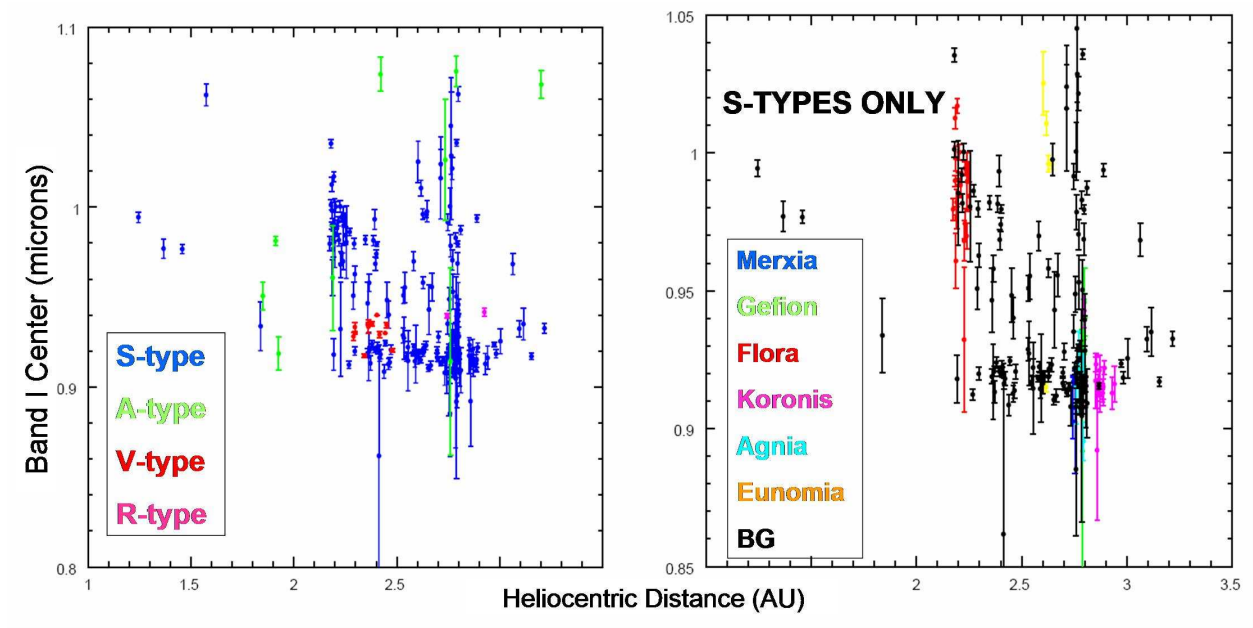


Fig. 3.— Heliocentric distribution. The left plot shows all asteroids divided by taxonomy. The right plot shows only S-types divided by family. We believe we are seeing a trend of decreasing olivine/pyroxene at higher heliocentric distances as evidenced by decreasing Band I Center wavelength.